

# Study on the Spatio-temporal Evolutionary Properties of Gas-liquid Two-phase Flow in Centrifugal Pump as Turbine (PAT)

J. Ying, H. Yang<sup>†</sup>, L. Li, X. Li, Y. Wei and Z. Zhu

Key Laboratory of Fluid Transmission Technology of Zhejiang Province, Zhejiang Sci-Tech University, Hangzhou, Zhejiang 310018, China

<sup>†</sup>Corresponding Author Email: [yanghui@zstu.edu.cn](mailto:yanghui@zstu.edu.cn)

## ABSTRACT

With the increasing complexity of the industrial production process, the transmission medium of the hydraulic turbine is no longer satisfied, and the gas-liquid two-phase mixed medium has to be considered. The presence of gas in the transmission medium will alter the internal flow structure of the hydraulic turbine and affect its operational stability. Therefore, for the purpose of clarifying the influence of inlet gas content on the internal flow of PAT, the unsteady flow of the PAT is simulated in this paper using numerical simulation. Based on the numerical simulation results, the influence of inlet gas content on the internal flow characteristics, characteristics of pressure fluctuation in impeller and volute, and vortex evolution of flow field are analyzed. The accumulation of gas phase leads to the emergence of vortices, and regions with low pressure values appear at the vortex generation. The major factor of the periodic variation of pressure fluctuation between volute and cut-water is the dynamic and static interference of impeller. The increase of gas content causes more flow disorder in the cut-water region and the volute contraction section. Since the gas in the flow channel is predominantly on the suction side of blades, the flow field on the suction side is more complex than that on the pressure side, and the amplitude of pressure fluctuation increases appropriately. The vortex structure is mainly distributed on balance hole, inlet area of impeller and suction side of blade. As the blade rotates, there are new shedding and growth of vortices, and finally attached to the volute wall. Increasing gas content enhances the influence of blade rotation on the vortex evolution characteristics in the volute and impeller.

## Article History

Received December 29, 2023

Revised May 16, 2024

Accepted May 27, 2024

Available online September 1, 2024

## Keywords:

Centrifugal pump as turbine

Gas-liquid two-phase flow

Spatio-temporal evolutionary

Pressure fluctuation

Vortex structure

## 1. INTRODUCTION

Hydraulic turbine is a kind of machine with high pressure fluid as working medium for energy conversion. It converts the pressure energy of high-pressure fluid into the rotating mechanical energy of the hydraulic turbine impeller. Centrifugal pump as turbine (PAT) is a centrifugal pump that operates in reverse under the action of high-pressure fluid, which is broadly accepted as a proper renewable generation tool (Kandi et al., 2022). Operating a centrifugal pump as a turbine emerges as a prime solution for small and micro-hydro power generation, effectively meeting energy requirements. (Adu et al., 2020; Achitaeve et al., 2022; Lu et al., 2022). With the development of industry, the fluid medium of hydraulic turbine is becoming more and more diversified. The medium can be single-phase water, liquid hydrogen, liquid oxygen, etc. Additionally, it can also be gas-liquid two-phase or even gas-liquid-solid three-phase. (Wu & Xue, 2021; Yang et al., 2022b; Chehadch et al., 2023). On

real industrial situations where PATs are currently operated by gas-liquid media with significant gas contents. For instance, in natural gas purification devices, the medium in the turbine is amine liquid rich in hydrogen sulfide mixed with bubbles.

Various unsteady conditions that may be encountered in the actual operation of PAT. Studying the unsteady spatio-temporal evolution of PAT assists in evaluating the stability of the system and prevent performance degradation or failure caused by unsteady characteristics. The unsteady properties of turbomachinery have been studied by some scholars. Zhang et al. (2022) and Ouyang et al. (2021) investigated the effect of impeller blade number and blade inclination angle on the pressure fluctuation of hydraulic turbine when centrifugal pump was used as turbine. Yang et al. (2022a) studied the vortex structure and pressure variation with an axial flow pump as a turbine by transient numerical simulation method. It was noted that the vortex rope rotation frequency gradually increased the pressure fluctuation in the dustpan-shaped duct with increasing distance from the

impeller. Lin et al. (2022) investigated the influence of impeller rotation on vorticity distribution and pressure fluctuation in volute. They established a relationship between vortex evolution and pressure fluctuation. Si et al. (2023) conducted entropy generation analysis and pressure fluctuation characteristics analysis of unsteady cavitation flow fields in centrifugal pumps. Feng et al. (2023) examined cavitation images on turbine components and pressure fluctuation on draft tubes under different cavitation conditions, noting significant dependence on cavitation state. Shi et al. (2019, 2021) and Chai et al. (2022) studied the effect of gas on PAT efficiency and operational stability under pure liquid phase and gas-liquid two-phase conditions. They observed a trend of decreasing then increasing dominant frequency amplitude of radial force with increasing gas content. The release of gas from the fluid during expansion leads to an increase in flow rate, delivering additional energy compared to incompressible flow (Stefanizzi et al., 2018). It is of great significance to study the gas-liquid two-phase flow problem and the flow characteristics and mechanism of turbine gas-liquid two-phase medium in the transport process (Li et al., 2019; Liu et al., 2019; Qin et al., 2022).

When the PAT is used for energy recovery of gas-liquid two-phase medium, the increase of gas content will have a great influence on the internal flow characteristics and mechanism. However, there is a notable lack of research concerning turbines operating under conditions characterized by high gas content at the moment. In addition, the study of the temporal and spatial development of instability of PAT under gas-liquid two-phase conditions helps to assess its stability and prevent performance degradation or failure due to unstable characteristics. Therefore, in this paper, the numerical simulation of PAT under high gas content conditions is carried out, and the temporal and the spatio-temporal evolutionary properties of gas-liquid two-phase flow are studied in depth. A detailed investigation is performed on the internal flow pattern, pressure fluctuation and vortex structure evolution of the PAT with gas-liquid two-phase flow. It aims to comprehensively analyze the evolution of the PAT flow properties, and the results are an important reference for improving the performance of PAT design.

## 2. GOVERNING EQUATIONS AND NUMERICAL METHOD

Due to the two-phase gas-liquid flow, the continuity and momentum equations used in this paper can be expressed as:

$$\frac{\partial(\alpha_k \rho_k)}{\partial t} + \nabla \cdot (\alpha_k \rho_k \mathbf{u}_k) = 0 \quad (1)$$

$$\frac{\partial(\alpha_k \rho_k \mathbf{u}_k)}{\partial t} + \nabla \cdot (\alpha_k \rho_k \mathbf{u}_k \mathbf{u}_k) = -\alpha_k \nabla P - \nabla \cdot \alpha_k \boldsymbol{\tau}_k + \alpha_k \rho_k \mathbf{g} + \mathbf{F} \quad (2)$$

where subscript  $k$  represents  $k$ -phase,  $\alpha$  is the volume fraction,  $\boldsymbol{\tau}$  is the stress tensor and  $\mathbf{F}$  is the momentum exchange between phases (Deen et al., 2001).

Euler-Euler multiphase flow model can be categorized into homogeneous flow and inhomogeneous model. In contrast to the homogeneous flow model, the inhomogeneous model treats each component separately and considers interphase transfer and interphase forces.



Fig. 1 Single-stage cantilever PAT

Table 1 Main geometric parameters of PAT

Parameters	Value
Rotational speed, $n$ (rpm)	2900
Design flow rate, $Q_d$ (kg/s)	22.43
Inlet diameter, $D_1$ (mm)	86
Outlet diameter, $D_2$ (mm)	169
Volute base diameter, $D_3$ (mm)	173
Impeller inlet width, $b_1$ (mm)	14
Impeller outlet width, $b_2$ (mm)	26
Blade inlet installation angle, $\beta_1$ (°)	33
Blade outlet installation angle, $\beta_2$ (°)	15
blade angle, $\varphi$ (°)	145
Number of blades	6

Therefore, the inhomogeneous model is selected for the study.

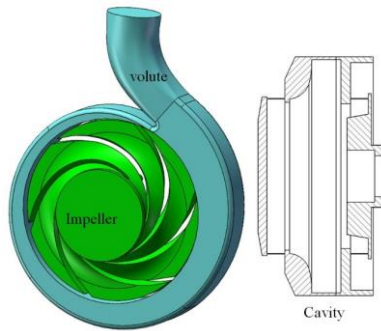
## 3. NUMERICAL SIMULATION AND EXPERIMENT

Single-stage centrifugal pump featuring a specific speed of 90 was reversed as a turbine to support our experimental investigation, as shown in Fig. 1. The primary geometric parameters of the PAT are given in Table 1.

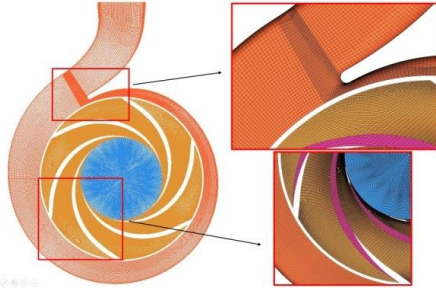
### 3.1 Computational Model and Grids

As shown in Fig. 2a, the model of PAT is divided into six parts: inlet, volute, impeller, front cavity, back cavity and outlet. The inlet and outlet of the PAT are properly extended in order to make the gas and liquid fully mixed and developed. Global structural mesh of the model was generated in ANSYS-ICEM, and the structural mesh of the impeller and volute is presented in Fig. 2b.

For an accurate simulation of turbulent flow, grids near the wall of the PAT is appropriately densified in the direction perpendicular to the wall. The wall average  $y^+$  value of each hydraulic component in PAT is illustrated in Table 2. Taking the efficiency of PAT under the design condition as the criterion, six groups of different numbers of grids are selected to verify the independence of the grids. As shown in Fig. 3, when the grid quantity is higher than  $5.2 \times 10^6$ , the efficiency of the PAT remains stable. Therefore, the final computational domain mesh number  $5.2 \times 10^6$  is selected is the simulation.



(a) three-dimensional model of PAT



(b) structural mesh of PAT

**Fig. 2 Models and Grids**

**Table 2 The average surface  $y^+$  value of each hydraulic component**

inlet	volute	impeller	front cavity	back cavity	outlet
5.41	31.42	16.24	6.54	4.84	5.36

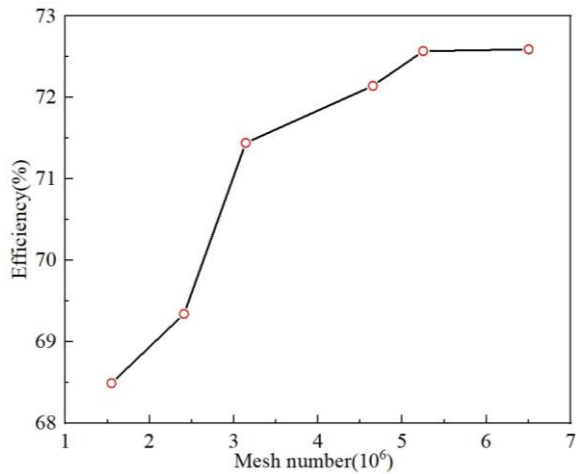


**Fig. 3 Efficiency of PAT with different mesh number**

### 3.2 Numerical Parameters

ANSYS-CFX is employed to perform numerical simulation for the PAT in this investigation. Based on the calculation of PAT with pure water as medium, we carried out the research on gas-containing condition of PAT. Non-slip boundary conditions at all of the stationary and rotating walls are applied. The transient rotor stator model is used to achieve data transmission the rotating domain

**Table 3 The value of the outlet pressure for all CFD tests**

Mass flow rate Q(kg/s)	Outlet pressure P <sub>2</sub> (MPa)
10.80	0.480
11.91	0.460
14.12	0.405
15.79	0.355
17.45	0.285
20.49	0.150
22.43	0.055
24.26	0.050
26.86	0.060

and the stationary domain. The boundary conditions on the inlet and outlet are mass flow rate and pressure. The value of the pressure imposed at the outlet for numerical simulations are according to the results given by the pressure gauge in the experiment. The value of the outlet pressure for all CFD tests are shown in Table 3. The turbulence model used in liquid phase is  $k-\omega$  SST model, while the model used in gas phase is zero-equation theoretical model. The liquid phase is an incompressible continuous phase, and the gas phase is an incompressible dispersed phase. The Schiller Neumann model is employed for momentum transfer. The gas enters the PAT uniformly as spherical bubbles with a diameter of 0.01 mm. The inlet gas content is set to 5%, 15%, 30% and 45%, respectively. Unsteady simulations are carried out with a time step of  $1.15 \times 10^{-4}$ s corresponding to 1/180 of the rotating cycle under the design condition based on stable steady simulation results. (Osman et al., 2022). The numerical results for the last rotation is mainly studied after a total time for 10 rotations of the rotating impeller is calculated.

### 3.3 Experiment Validation of Pure Water

The experimental investigation was carried out in a company in Hangzhou. The schematic diagram of the turbine experimental system is depicted in Fig. 4. After the water tower storage is completed, the fluid is pressurized by a booster pump, and the generated high-pressure liquid drives the impeller of PAT to rotate at a high speed. The rotational speed and output torque of the PAT are

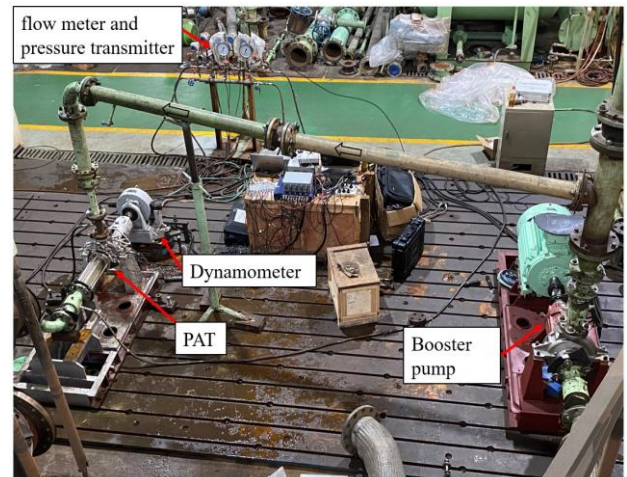


**Fig. 4 The PAT test system**

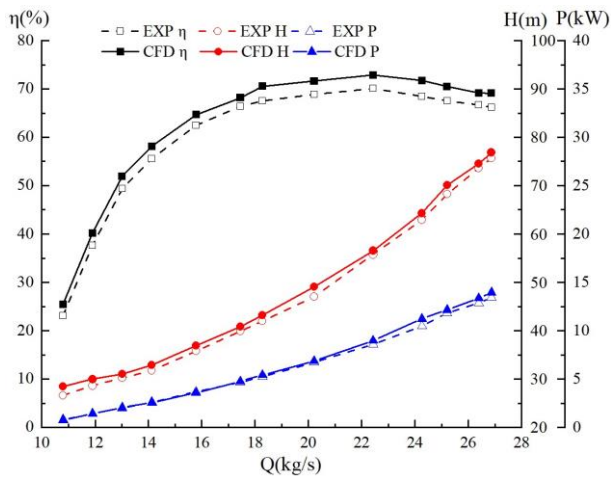


**Fig. 5 Comparison of experimental and simulation results of head, efficiency and shaft power for PAT**

measured by a dynamometer connected to the PAT. The flow rate is measured by the inlet section flow meter, and the pressure is recorded by the pressure transmitter at the inlet and outlet of the PAT. The performance parameters such as head, efficiency and shaft power of the PAT can be calculated from the basic parameters collected and measured. Based on the performed experiments and investigating the results of the extracted experimental data, the measurement errors of flow in flow rate, pressure, dynamometer speed and dynamometer torque sensor are:  $\pm 0.5\%$ ,  $\pm 0.4\%$ ,  $\pm 0.2\%$ ,  $\pm 0.4\%$ , respectively. These deviations can be produced by the measurement uncertainties.

The comparison of experimental and numerical values of the head and efficiency are illustrated in Fig. 5. It is found that the performance curve trends of numerical simulation results and experimental results are basically consistent. Experimental outcomes exhibit smaller values compared to the numerical simulation results. The reason can be the structural simplification of some parts in the CFD simulation, on the other hand, taking into account some of the flow losses without considering leakage and mechanical losses. However, the value of uncertainty of the relative errors of efficiency, head and shaft power in the experiment and numerical simulation are  $(4.8 \pm 1.9)\%$ ,  $(3.1 \pm 1.6)\%$  and  $(1.6 \pm 3.7)\%$ , respectively. The error is within the acceptable range. Therefore, the numerical calculation method is feasible.

### 3.4 Validation of Gas-Liquid Two-Phase Model

For the purpose of validating of the Euler-Euler two-fluid model's accuracy in the gas-liquid two-phase flow calculation, the experimental results of gas-liquid two-phase flow in a three-dimensional square column by Deen et al. (2001) were utilized. The geometry of the 3D square column computational domain is shown in Fig. 6. The square column is filled with water and gas entering from the bottom at a speed of 0.0784 m/s. A straight line at a height of 0.25 m in the column's center was used by Deen to measure the axial liquid velocity, resulting in the axial liquid velocity distribution at this height. The SST  $k-\omega$  turbulence model is applied to the liquid phase, while zero-equation model is employed for the gas phase. The

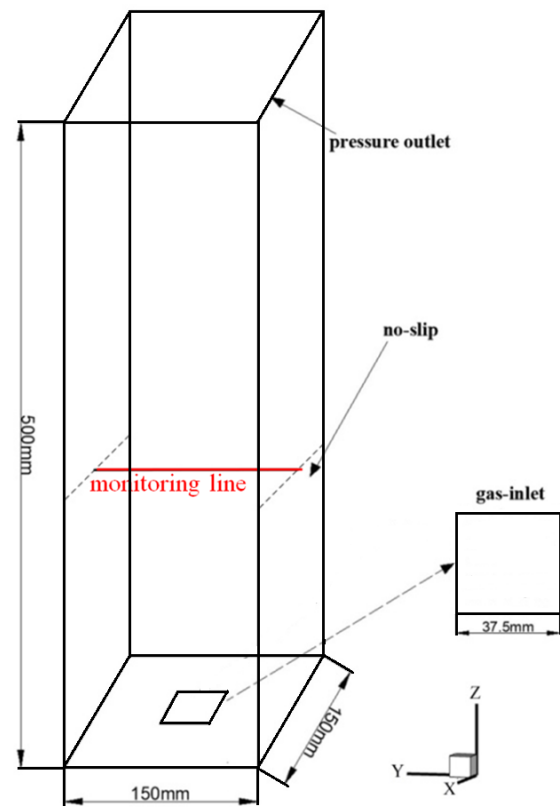


**Fig. 6 Model of the square column and schematic of the monitoring line**

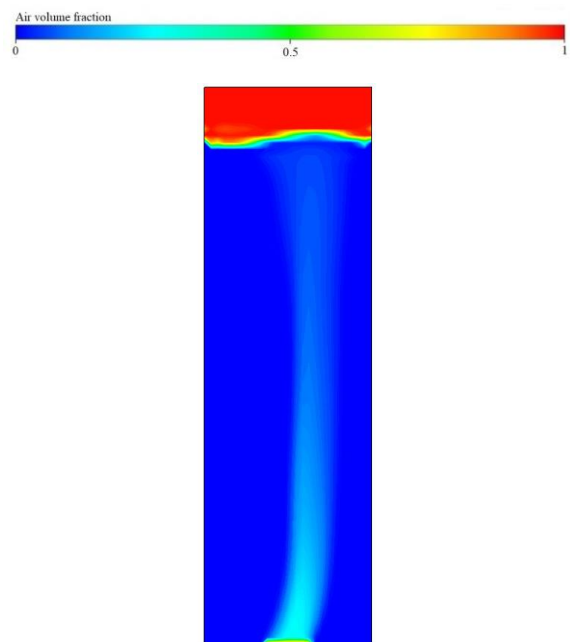


**Fig. 7 The void fraction distribution of the square column**

unsteady simulation with a time step of 0.01s and a total calculation time of 150s. Analysis is focused on the results from the last 50s of stabilized gas-liquid two-phase flow.

The void fraction distribution of the square column is shown in Fig.7. At this moment, the airflow can be seen to be deflected in the square column.

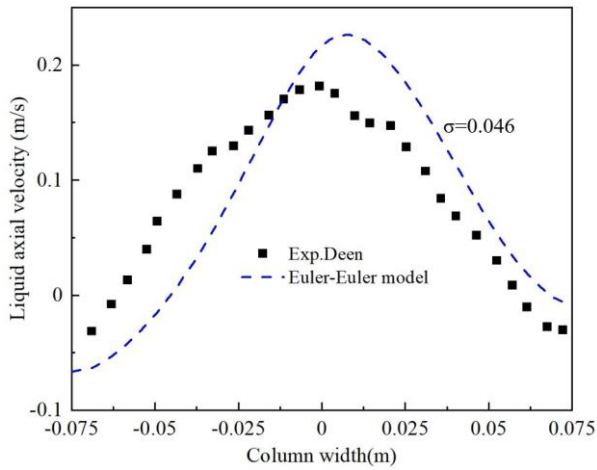


**Fig. 8 The axial velocity distribution of the liquid phase at the monitoring line**

Figure 8 shows the axial velocity distribution of the liquid phase at the monitoring line. The standard deviation between the simulation results obtained by the two-fluid model and the experimental is 0.046. It can be concluded that the simulation results are in general agreement with the experimental trends.

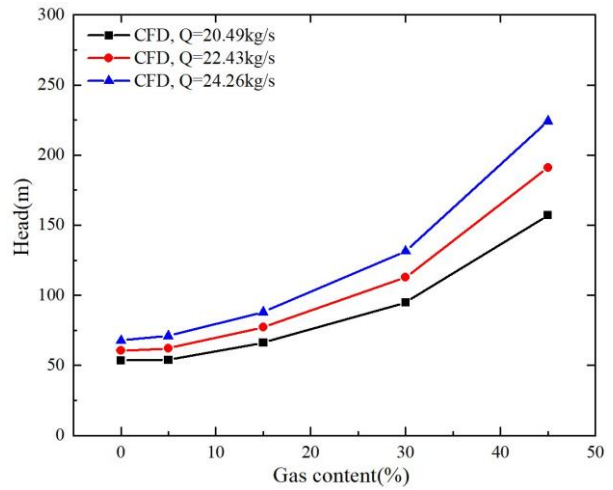
In addition, according to the study of gas-liquid two-phase pump by Minemura et al., it is found that the two-fluid model still has certain accuracy under the influence of impeller rotation. Therefore, it is feasible to employ the two-fluid model to the study of gas-liquid two-phase flow in PAT (Mikielewicz et al., 1978; Furuya, 1985; Minemura et al., 1998).

## 4. RESULT AND DISCUSSION

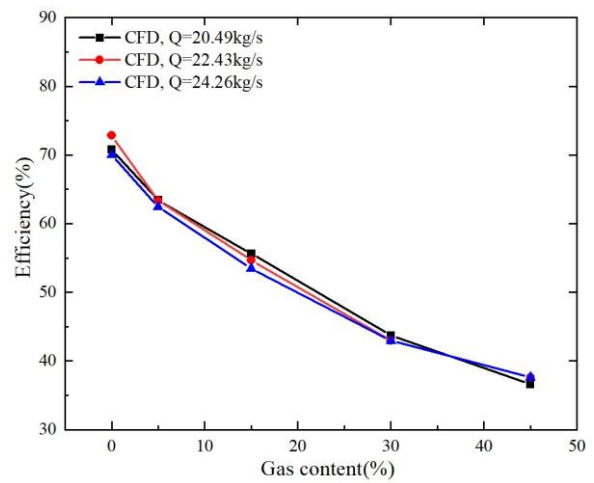
### 4.1 The Performance Modifications of PAT under Different Gas Content

Studying the performance changes of gas-liquid two-phase hydraulic turbines under different gas contents is of great significance for improving equipment efficiency and adapting to different working conditions. The values of head, shaft power and hydraulic efficiency of the simulated PAT under different gas content and different flow conditions are presented in Fig. 9.

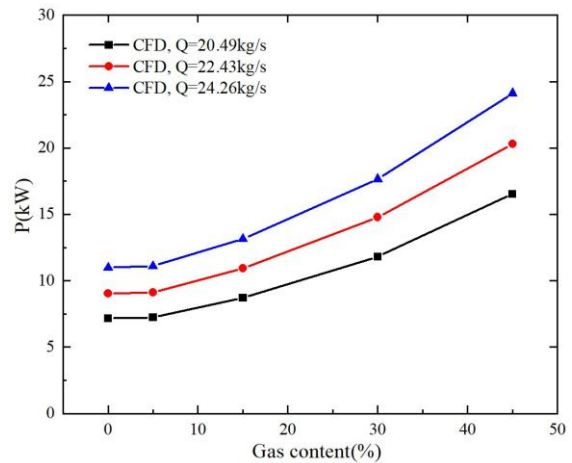
According to Fig. 9a and Fig. 9c, at the same flow rate, the head and shaft power curves of PAT show an upward trend with the increase of gas content. At the same gas content, increasing the flow rate leads to an increase in head values and shaft power. Since the flow rate increases, the work applied to the impeller also increases, thereby increasing the head and shaft power. When the gas content increases from 5% to 45%, the head and shaft power of the low flow rate condition increase by 191.4% and 128.5% respectively, the head and shaft power of the design flow rate condition increase by 212.8% and 122.5% respectively, and the head and shaft power of the high flow rate condition increase by 215.7% and 117.5% respectively. In Fig. 9b, with the gas content increases, the hydraulic efficiency of PAT decreases. Under the condition of pure water, the efficiency is the highest when the flow rate is  $Q=22.43\text{kg/s}$  (design flow rate). As the gas



(a)head



(b)efficiency



(c)shaft power

**Fig. 9 Performance curves of PAT with different gas content**

content increases, the efficiency decreases, and the efficiency of small flow gradually exceeds the design flow. When the gas content increases to 15%, the efficiency of small flow is the highest. At high gas content (45%), the efficiency of high flow rate is higher than that of low flow rates. The reason for this change may be related to the

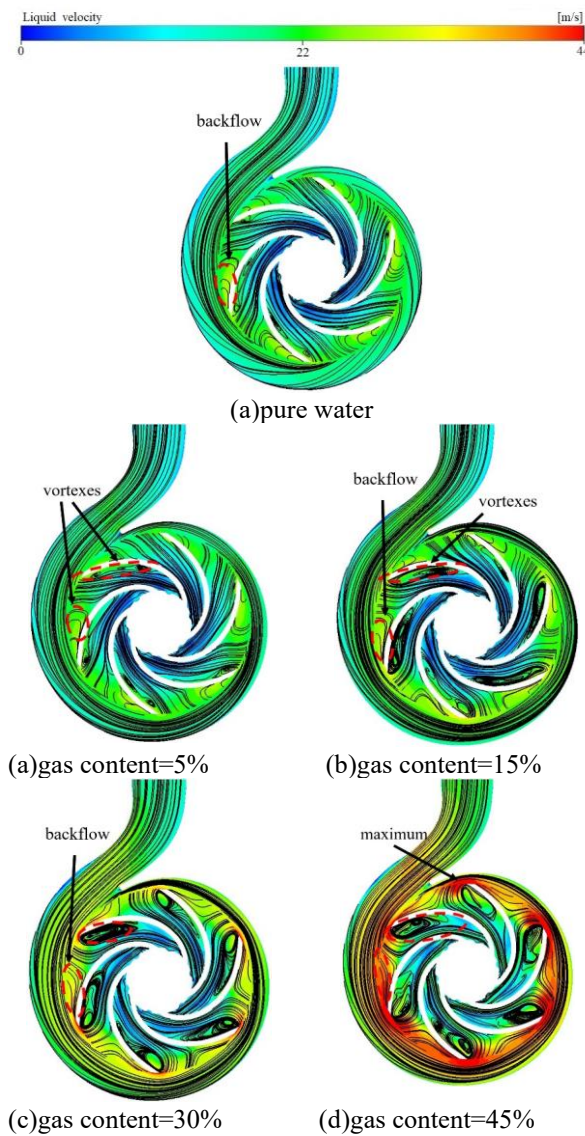


**Fig. 10** Distribution of streamlines in volute and impeller with different gas content

influence of the increase of gas content on the internal flow under different flow rates. In addition, with the increase of gas content, the growth rate of head is significantly higher than that of shaft power, which means that the output power increases slower than the input power. This leads to an increase in the head and shaft power of the PAT while accompanied by a decrease in the efficiency of the PAT.

#### 4.2 Influence of Gas Content on Internal Flow Characteristics of PAT

The volute and impeller are important flow passage components of the PAT. As the fluid moves from the volute to the impeller, the flow field will become more complex, so the distribution of streamlines in the impeller and volute is studied. Figure 10 displays the streamline distribution of liquid in the impeller and volute under different gas content. According to Fig. 10, it can be seen that the velocity in the volute is significantly greater than the velocity in the impeller. This is attributed to the conversion of kinetic energy and pressure energy to the mechanical energy of the impeller as the fluid enters the impeller from the volute. From Fig. 10a, under the condition of pure

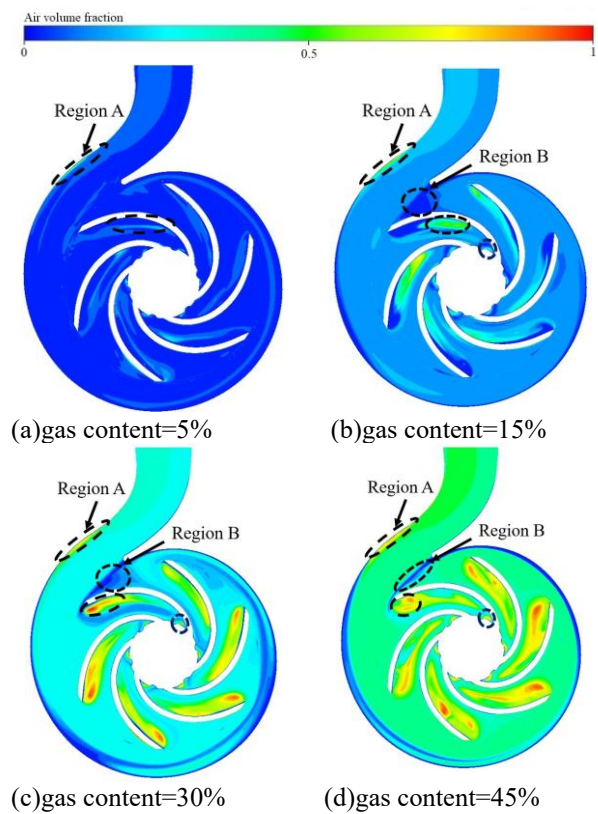


**Fig. 11** Gas distribution in impeller with different gas content

water, the vortex is very few and the streamline is more orderly. Backflow is observed in the impeller inlet region. With the increase of gas content, the streamlines in each flow channel of the impeller are relatively disordered. Vortexes are formed with minimum velocity in each flow channel of impeller. From 5% to 15%, the vortex size of each flow channel in the impeller increases. When the gas content increases to 30%, it is noteworthy to mention that the velocity maximum occurs at the gap between the volute and the blades. When the gas content increases to 45%, the diameter of the vortex in the flow channel increases further, occupying 2/3 of the flow channel. These vortexes lead to more serious blockage in the flow channel and increase energy loss, resulting in a decrease in the efficiency of PAT.

Turbulence characteristics within the volute and impeller flow field may be related to the interaction between the gas and liquid phases. Thus, the gas distribution in the impeller and volute under different gas content is illustrated in Fig. 11. The gas is mainly concentrated on the walls of the cut-water (in region A) and the suction side of the blade. With the increase of gas content, the gas volume fraction in each flow channel of the impeller increases obviously, and the area of the gas phase region increases. The reason can be attributed to the centrifugal force during the rotation of the impeller, which causes the gas to accumulate on the suction side of blade. It gradually moves along the suction side towards the inlet of the impeller channel. In addition, influenced by the volute structure, significant gas-liquid separation is observed at the cut-water of the volute (in Region B), where the liquid phase converges.

Considering the characteristics of gas-liquid two-

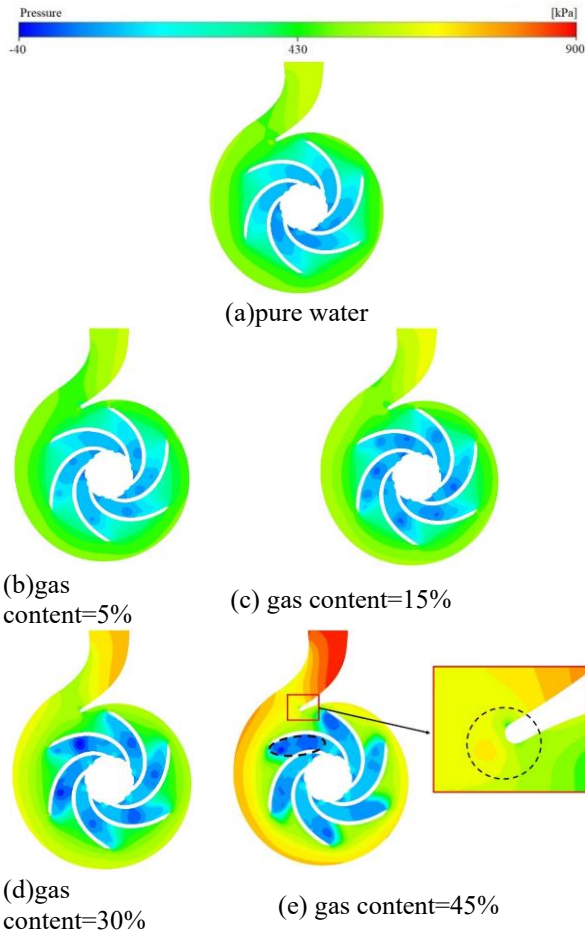


**Fig. 12 Pressure distribution in impeller and volute with different gas content**

phase flow, the pressure distribution may become uneven due to the presence of gas. The accumulation of gas may lead to the pressure increase or decrease at the local region. In Fig. 12, comparison between the contours of pressure in the volute and impeller is performed with different gas content. Under pure water condition (see Fig. 12a), it is found that the pressure value decreases along the direction of fluid flow. The maximum value of pressure is observed at the inlet of the volute, and the pressure at the outlet of the impeller is the smallest. At 5 % gas content, the area of low pressure begins to appear in the middle of the blade channel. With the increase of the gas content, the area of low pressure gradually shifted to the impeller inlet. The reason for this phenomenon may be that when the gas content is low, the distribution of gas and liquid phase exhibit a more uniform distribution within the impeller. But with the increase of gas content, the interaction between gas and liquid phases is intensified, which leads to the complexity of the flow. The accumulation of gas phase leads to the emergence of vortices, and regions with low pressure values appear at the vortex generation. In particular, the pressure distribution in the cut-water area is quite different, which can be explained by the large pressure between the impeller and the cut-water caused by the impact of the gas-liquid mixture on the cut-water.

### 4.3 Analysis of Pressure Fluctuation Characteristics

The pressure fluctuation signal is usually closely related to the vortex structure and vorticity evolution. The vortex can be regarded as the rotation of the fluid velocity,

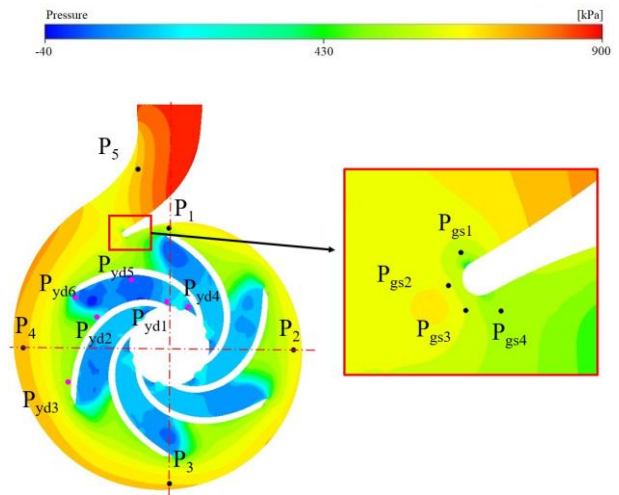


**Fig. 13 Monitoring points distribution**

which is usually formed in the place where the velocity gradient in the fluid is large. The change of the vortex structure and vorticity can lead to the disturbance of the fluid velocity field. These disturbances will cause pressure changes in the flow field, resulting in pressure fluctuation signals. The pressure fluctuation characteristics in volute and impeller under different gas content are studied emphatically. According to the pressure distribution in Fig. 12 (d), monitoring points are set up in the area with large pressure gradient, to visually display the change of pressure with time and frequency. Various monitoring points are established within the impeller channel, volute circumferential and cut-water area to monitor the pressure fluctuation at each moment. The specific monitoring point location distribution is presented in Fig. 13. Four points ( $P_{gs1} \sim P_{gs4}$ ) are set in the cut-water area. Five points are arranged at the out-wall of the volute circumference, which are  $P_1, P_2, P_3, P_4,$  and  $P_5,$  respectively. Meanwhile, six points ( $P_{yd1} \sim P_{yd6}$ ) along the suction and pressure sides of blades are uniformly arranged to investigate the pressure fluctuation in the impeller channel. It is worth noting that since the impeller is set to the rotating domain, the monitoring points on the blade channel are also dynamic.

After ensuring the stability of the PAT operation, the analysis focus on the pressure fluctuation characteristics according to the last rotation period of the impeller. The theoretical shaft frequency  $f_R$  is 48.3Hz.

In order to compare the results more intuitively, the specific pressure value is transformed into the pressure fluctuation coefficient  $C_p$  by dimensionless treatment of the pressure. The coefficient of pressure fluctuation  $C_p$  is expressed as follows (Lin et al., 2022):

$$C_p = \frac{(P - \bar{P})}{0.5 \rho_m u_2^2} \quad (3)$$

Where,  $P$  represents the static pressure (Pa),  $\bar{P}$  is the time average pressure of monitoring point (Pa),  $\rho_m$  represents the density of the gas-liquid mixture ( $\text{kg/m}^3$ ), and  $u_2$  represents the circumferential velocity of the impeller outlet (m/s). Furthermore, Analysis of the pressure fluctuation spectrum at various monitoring points is conducted using the Fourier transform method.

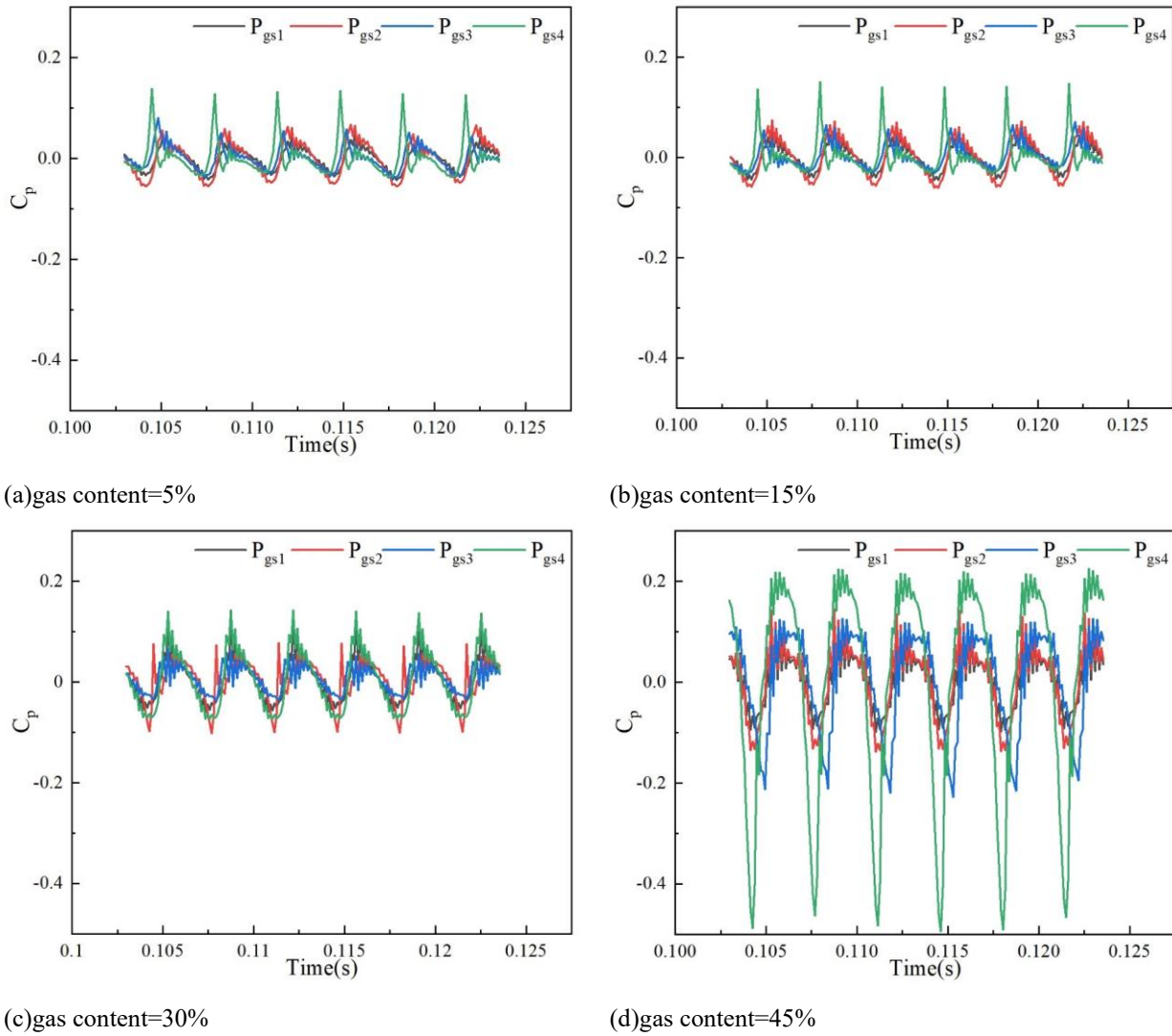


**Fig. 14 Time domain characteristic of  $C_p$  fluctuation at the cut-water**

### 4.3.1 Pressure fluctuation analysis of cut-water area

The time domain characteristic of the pressure fluctuation of the monitoring points ( $P_{gs1} \sim P_{gs4}$ ) in the cut-water area at different gas content is illustrated in Fig. 14. Observing the diagram reveals that the fluctuation law of pressure fluctuation coefficient is similar at different gas content, the peaks and troughs corresponding to the number of blades appear in each cycle. This shows that the reason for the fluctuation is mainly due to the dynamic and static interference between the rotating blade and the cut-water of the volute. Under the condition of low gas content (5 % and 10 %), the positive peak value of pressure fluctuation is greater than the negative peak value, and the positive peak value is about twice the negative peak value. When the gas content reaches 30%, the negative peak increased significantly to be equal to the positive peak. It is worth noting that at 45 % gas content, The negative peak of  $P_{gs4}$  is about twice the positive peak. This shows that the increase of gas content results in more flow disorders and backflow in the cut-water area, especially in the volute contraction section. The pressure fluctuation at  $P_{gs4}$  is the most pronounced, surpassing the amplitudes at other points. The reason can be explained by that the  $P_{gs4}$  is set in the contraction section with large curvature of the volute, where the gap between the

impeller and the volute is small, and the velocity gradient of the fluid changes greatly, resulting in strong pressure fluctuation here.

Based on the analysis of the pressure fluctuation at the monitoring points, the frequency domain characteristics are further investigated by Fast Fourier Transform (FFT), and the results are shown in Fig. 15. The main frequency observed at every monitoring point is 6 times  $f_R$ , that is, the frequency of the high frequency is the blade frequency. The frequency domain characteristic shows that the blade frequency is still the dominant frequency, which is related to the interaction by rotor-stator. The amplitude of the main frequency pressure fluctuation attenuates step by step with the blade frequency. With the increase of gas content, the amplitude of pressure fluctuation increases gradually. The maximum value of the dominant frequency appears at  $P_{gs4}$  ( $C_p=0.26$ ) at 45% gas content. It is worth mentioning that compared with 30% gas content, the main frequency amplitude of  $P_{gs3}$  and  $P_{gs4}$  increased by 399.7 % and 1000.59% respectively when the gas content is 45%. This corresponds to the results of flow disturbance and backflow at point  $P_{gs4}$  in the time domain diagram.

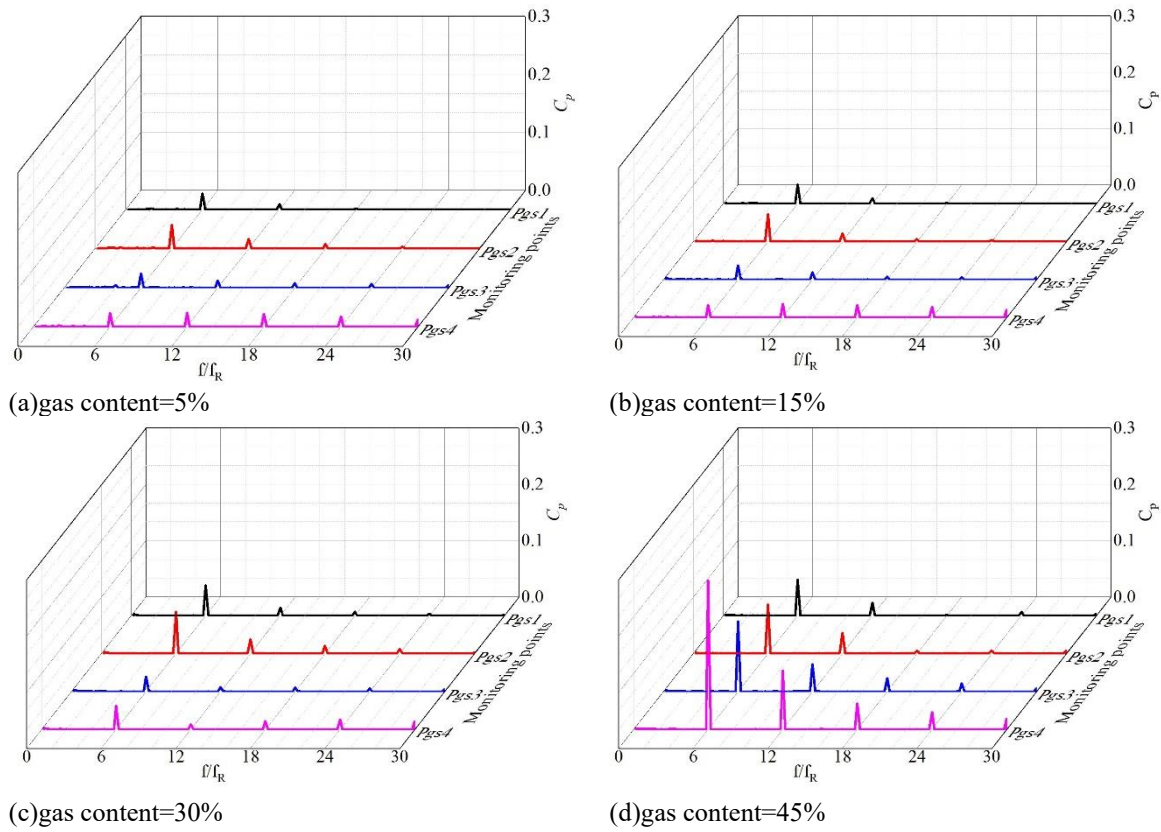


**Fig. 15** Frequency domain characteristic of  $C_p$  fluctuation at the cut-water

### 4.3.2 Pressure Fluctuation Analysis of Circumferential Volute

As depicted in Fig. 13, five monitoring points ( $P_1$ ,  $P_2$ ,  $P_3$ ,  $P_4$ ,  $P_5$ ) are set at varying positions along the circumferential direction of the volute to analyze the variation of the pressure fluctuation coefficient in the volute channel with time. Regarding the time domain characteristic (see Fig. 16), it is found that under different gas content conditions, the pressure fluctuations at each monitoring point in the circumferential direction of the volute show a periodic law, and each monitoring point has a peak and trough corresponding to the number of blades. In addition, the main pressure fluctuation amplitude of each monitoring point is different. At the point  $P_1$  near the cut-water, the amplitude of pressure fluctuation is notably higher compared to other points. The amplitude of pressure fluctuation at other monitoring points away from the cut-water is about 1/3 of that at point  $P_1$ . The reason can be attributed to two factors: firstly, because point  $P_1$  is located in the contraction section of the volute, the curvature is large, and there may be backflow, which leads to the enhancement of flow disorder. Secondly, the dynamic and static interference near the cut-water is greatly affected. From the comparison of pressure fluctuation amplitude under varying gas content conditions, with the increase of gas content, the fluctuation amplitude of  $C_p$  at each monitor increase. An increase in the amplitude of  $P_1$  is particularly obvious when the gas content is 45%, which is about twice that when the gas content is 5%. It is evident that an increase in gas content leads to enhanced flow instability within the volute.

Figure 17 depicts the frequency domain characteristic of pressure fluctuation in the circumferential volute with varying gas content. It is found that the frequency of the maximum pressure fluctuation at each monitoring point is the blade frequency and its harmonic frequency, and the pressure fluctuation at the blade frequency plays a leading role. Therefore, the main reason for the periodic variation of the circumferential pressure fluctuation in the volute is the static and dynamic interference of the impeller. Remarkably, there is a broadband fluctuation region in the low frequency band, which may be caused by some complex flows. It can be quantitatively seen that when the gas content is increased from 5% to 45%, the amplitude of  $P_1$ ,  $P_2$ ,  $P_3$ ,  $P_4$  and  $P_5$  points increased by 139%, 72.42%, 205.79%, 99.7% and 124.6% respectively. It can be concluded that the increase in gas content leads to an augmentation in circumferential pressure fluctuation in the volute, and the flow field in the volute is more unstable.

### 4.3.3 Pressure Fluctuation Analysis of Impeller Channel

The time domain characteristics of pressure fluctuation on the blade pressure side and the blade suction side with different gas content are shown in Figs. 18 and 19 respectively. It has been observed that the amplitude of pressure fluctuation increases with time. The reason can be explained as that in the period of one rotation of the impeller, the flow channel of the monitored impeller will gradually approach the contraction section of the volute, which will be affected by the structure of volute, resulting in the increase of pressure fluctuation in the blade passage with time. The frequency domain characteristic shows that the pressure fluctuation amplitudes of  $P_{yd1}$  and  $P_{yd4}$  are smaller than other

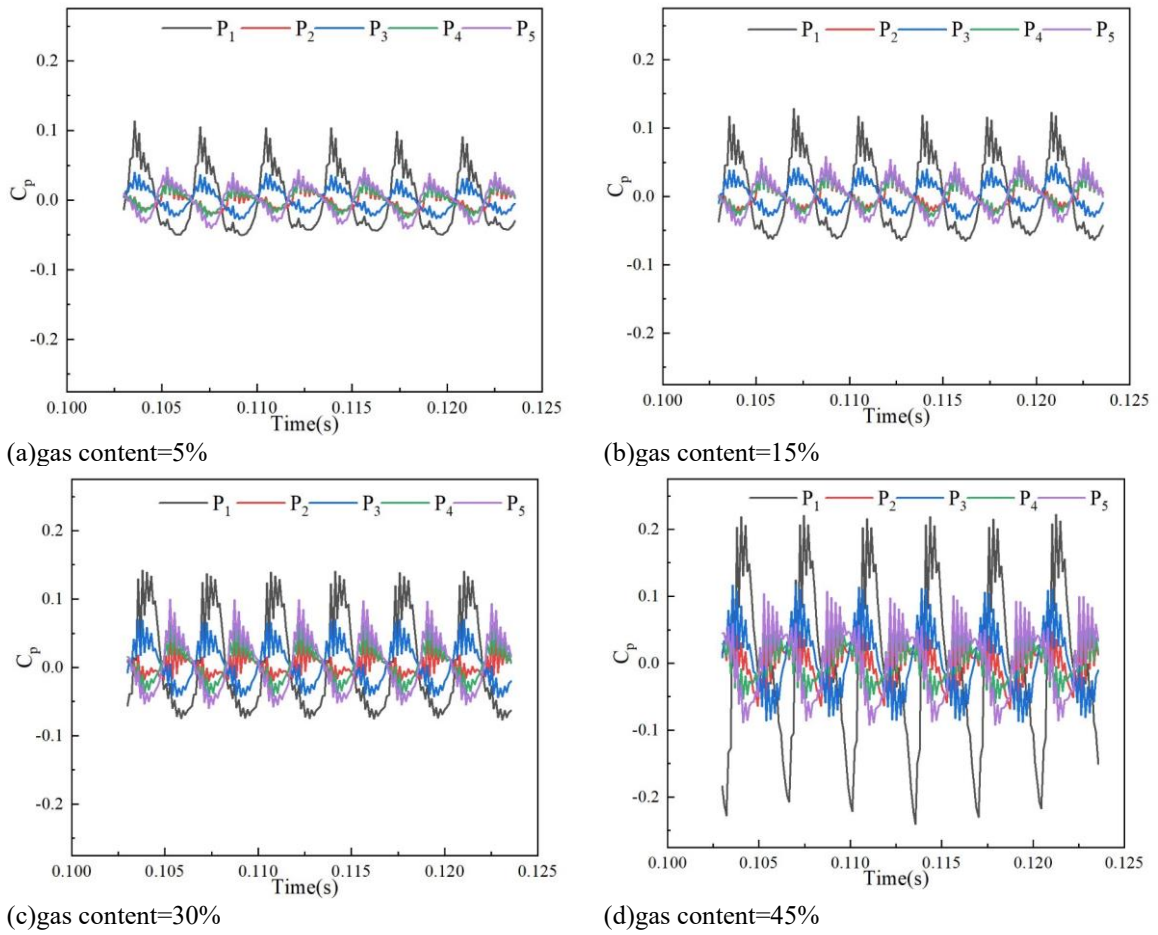


**Fig. 16** Time domain characteristic of  $C_p$  fluctuation in the circumferential volute

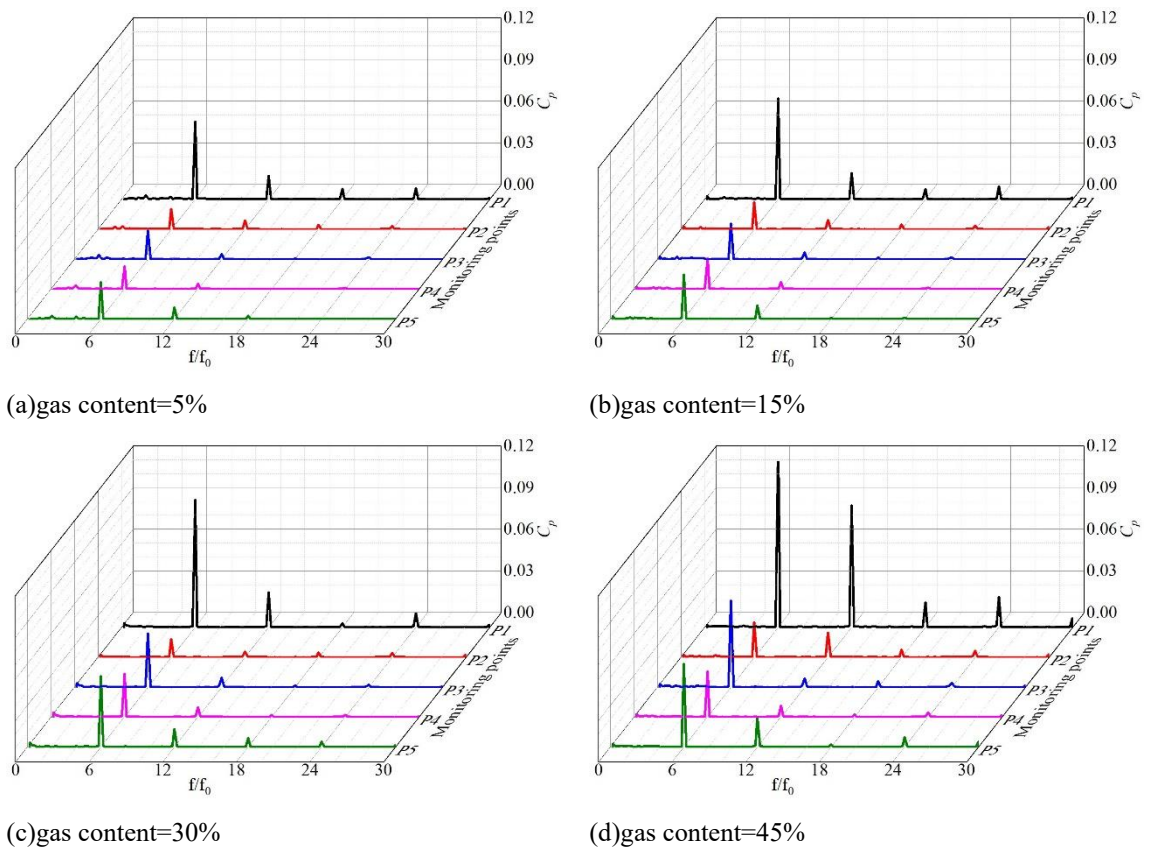


**Fig. 17** Frequency domain characteristic of  $C_p$  fluctuation in the circumferential volute

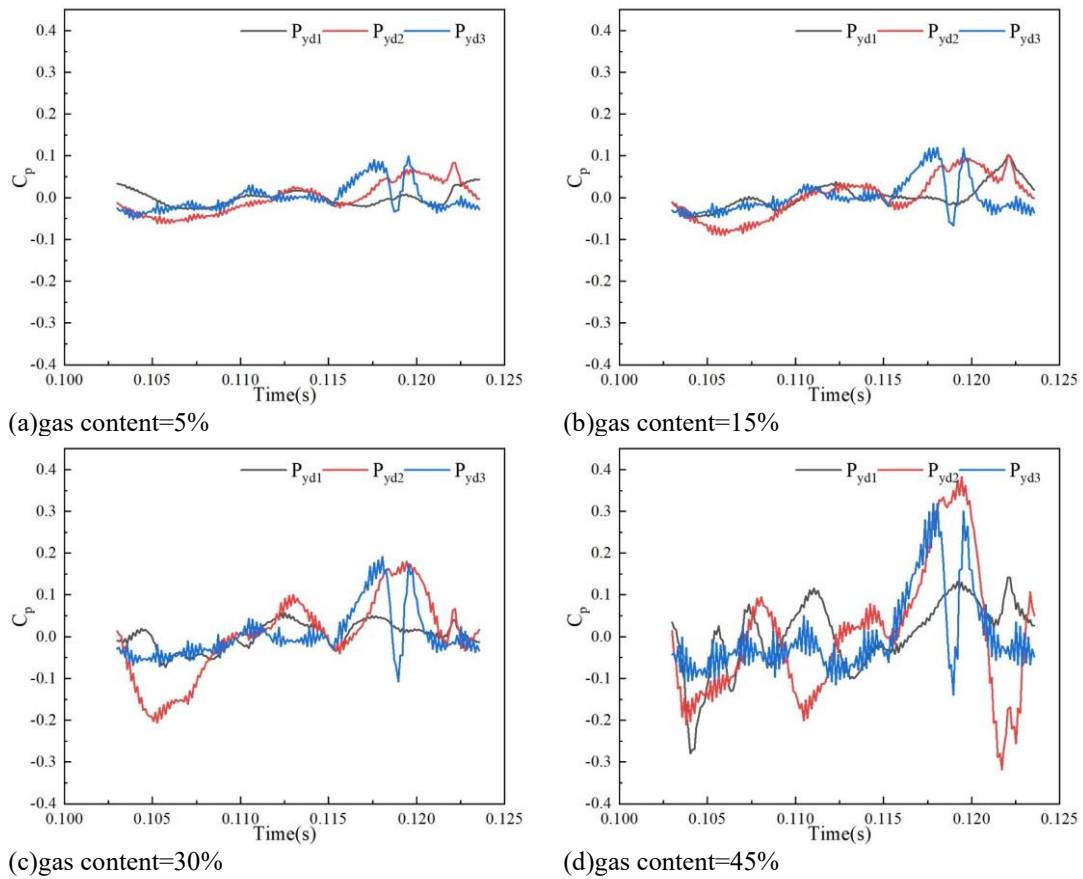


**Fig. 18 Time domain characteristic of  $C_p$  fluctuation in the pressure side of blade**

monitoring points. The reason can be attributed to that  $P_{yd1}$  ( $P_{yd4}$ ) is a monitoring point near the impeller outlet. The fluid flows from the volute to the impeller, passing through  $P_{yd3}$  ( $P_{yd6}$ ) and  $P_{yd2}$  ( $P_{yd5}$ ) in turn. When the flow reaches the  $P_{yd1}$  ( $P_{yd4}$ ) point, the flow field has stabilized. Comparing Fig. 18 and Fig. 19, it is revealed that the pressure fluctuation of the blade suction side appear to have a highly similarity to that of the pressure side, but the amplitude is different. The reason can be explained by that the gas phase in the flow channel is predominantly located on the suction side, the flow field on the suction side will be more complex than that on the pressure side, and the amplitude will increase appropriately. As shown in Fig. 19c and Fig. 19d, at high gas content, the gas phase at the monitoring points  $P_{yd5}$  and  $P_{yd6}$  has a significant accumulation phenomenon, and the gas-liquid two-phase flow separation phenomenon has intensified, causing a significant change in pressure fluctuation. Therefore, the increase of inlet gas content will have a significant impact on the stability of internal flow in PAT.

Characteristics of pressure fluctuation in the frequency domain with varying gas content Over the course of a single impeller rotation are illustrated in Fig. 20. The maximum fluctuation amplitude at 5 % gas content appears at the rotation frequency of  $P_{yd6}$  at the impeller inlet ( $C_p=0.058$ ), which is Approximately 3.5 times greater than the maximum peak value of  $P_{yd1}$  at the impeller outlet ( $C_p=0.017$ ). With the increase of gas content, the amplitude of  $P_{yd2}$  and  $P_{yd5}$  increases. When the gas content is 30 %, the maximum fluctuation amplitude is observed at the double frequency of the  $P_{yd2}$  ( $C_p=0.099$ ). When the gas content is 45 %, the maximum

fluctuation amplitude appears at 2 times the rotation frequency of the  $P_{yd6}$  point, and the amplitude of the monitoring points near the inlet is relatively large. The channel blockage in the inlet area caused by air mass agglomeration under high gas content conditions may be the reason for the high main frequency fluctuation of the inlet monitoring point. Therefore, the increase of gas content is the contributing factor to the increase of flow disorder. It is worth mentioning that the maximum fluctuation amplitude is mainly concentrated at the blade frequency of 1/3 of the impeller rotation. The reason for this phenomenon is that the impeller channel where the monitoring point is located is close to the cut-water, and the flow instability increases. As the flow channel is away from the cut-water, the amplitude of pressure fluctuation decreases gradually.

#### 4.4 Vortex Analysis of Volute and Impeller

##### 4.4.1 Spatio-Temporal Evolutionary Properties of Impeller Vortex Structure Distribution under Different Gas Content

The frequency and amplitude of the pressure fluctuation signal usually also reflect the characteristics of the evolution of the vortex structure. Combined with the analysis of the pressure fluctuation of the impeller, it can be inferred that the temporal and spatial evolution of the vortex structure is significantly influenced by gas content. The physical content of the Q criterion relates to the second invariant of the velocity gradient tensor. These regions are indicative of fluid flow structures that are susceptible to instability and turbulence. The relevance of the Q criterion lies in its ability to identify and characterize

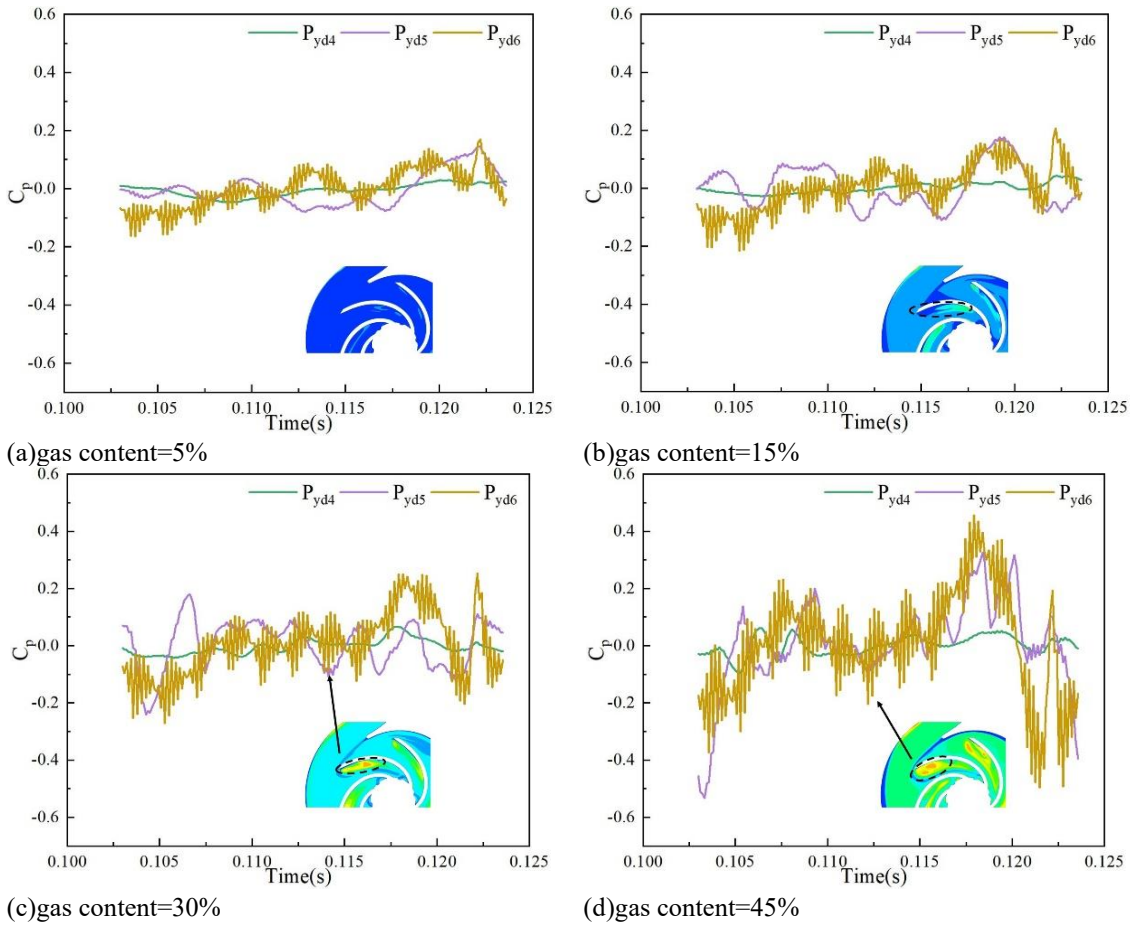


**Fig. 19 Time domain characteristic of  $C_p$  fluctuation in the suction side of blade**

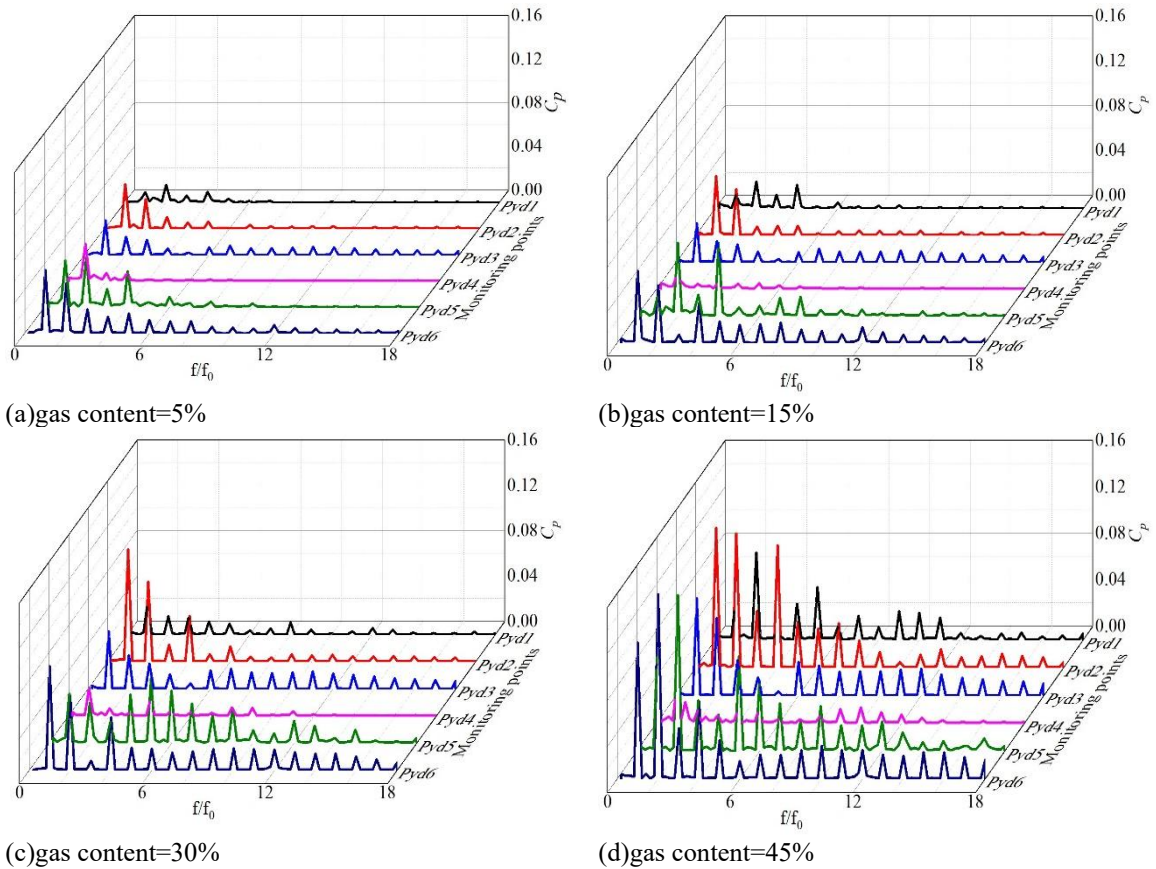


**Fig. 20 Frequency domain characteristic of  $C_p$  fluctuation in the impeller channel**

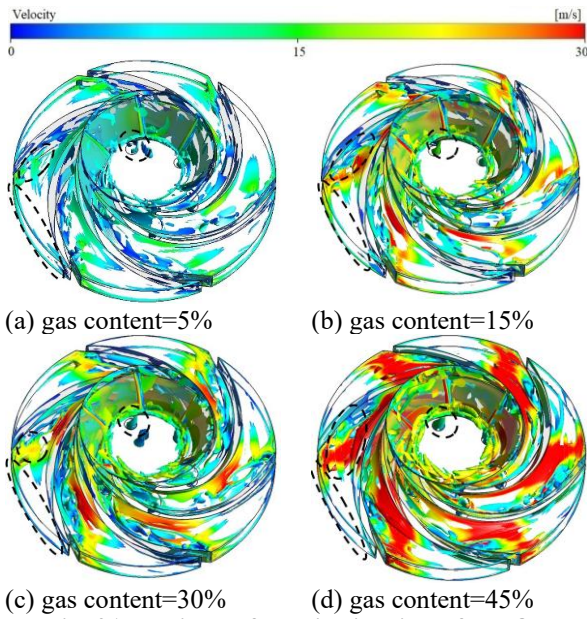


**Fig. 21 The isosurface distribution of the Q value with different gas content**

fluid flow features associated with turbulent behavior. Q criterion method is employed in this paper to analyze the vorticity of PAT impeller and volute (Hunt,1987; Bobba, 2006). The Q criterion is defined as:

$$Q = \frac{1}{2} [|\Omega|^2 - |S|^2] \quad (4)$$

Where  $\Omega$  means the rotation rate tensor, which can be obtained by:

$$\Omega = \frac{1}{2} [\nabla \mathbf{u} - (\nabla \mathbf{u})^T] \quad (5)$$

$$S = \frac{1}{2} [\nabla \mathbf{u} + (\nabla \mathbf{u})^T] \quad (6)$$

According to the definition of Q criterion, the numerical simulation flow field of the PAT under different gas content conditions is further processed, and the velocity flow field distribution is used as a variable to form the vortex structure distribution of PAT under the same Q value ( $Q=3 \times 10^6 \text{s}^{-2}$ ) with different gas content, as illustrated in Fig. 21. The velocity and vortex structure are interrelated and influenced each other. The fluid velocity is usually higher in the region with strong vortex structure. The internal vortex structure of the impeller is predominantly located on the blade suction side, the impeller inlet area and balance hole. The vortex structure located on the blade suction side is mainly caused by the viscous flow of the boundary layer on the blade wall. The reason for the vortex structure in the inlet area of the impeller can be explained by the backflow of the fluid in the inlet area of each blade channel of the impeller. The impact of fluid on the narrow structure of the balance hole can be reported as the reason for the generation of vortex structure in the balance hole. In addition, with the increase of gas content, the vortex intensity and vortex structure distribution area inside the impeller are significantly enhanced. It is indicated that the increase of gas content leads to more turbulent flow.

In conditions of low gas content, the vortex structure is sparse, resulting in a distinct distribution that allows for easier observation of temporal and spatial evolution

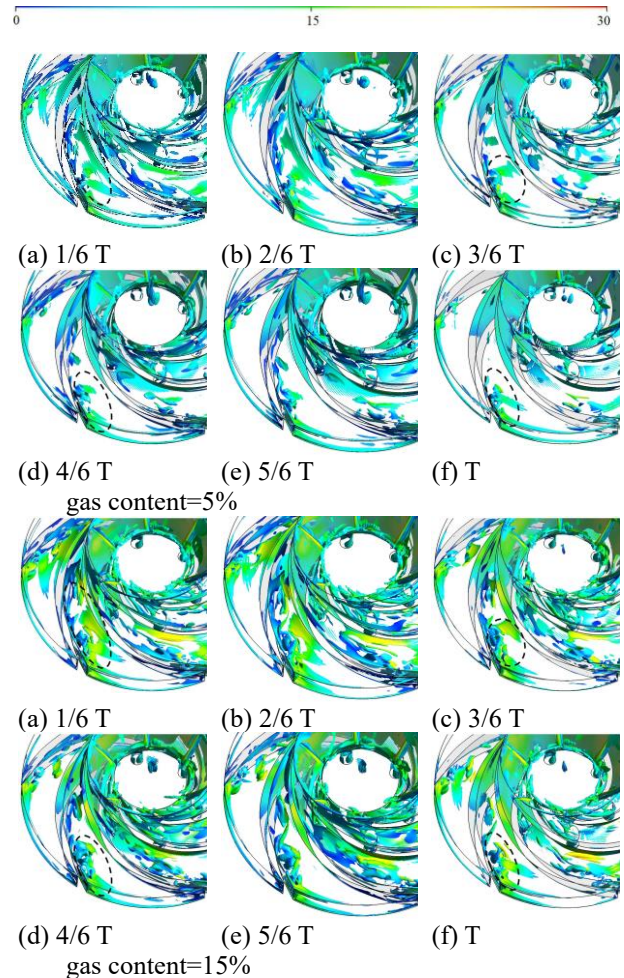


**Fig. 22 Vortex structure evolution of impeller with different gas content**

patterns. For the purpose of examining the influence of impeller rotation on the distribution of impeller vortex structure, the time evolution diagram of vortex structure distribution of impeller with low gas content in a rotation cycle is presented in Fig. 22. At 5% gas content, when the impeller turns 1/6 T, the area of vortex structure distribution is large and mainly concentrated on the blade suction side. When the impeller turns 3/6 T, the number of vortex structures in the impeller flow channel is significantly reduced until the impeller passes the whole cycle, and the vortex near the blade is completely concentrated at the blade leading edge. At 15% gas content, when the impeller rotates for 3/6 T, the vortex structure gradually moves along the blade suction side to the direction near the impeller inlet. When the impeller turns 4/6 T, the vortex structure is broken, and the small-scale vortex structure is spread on the suction side. When the impeller turns one cycle, the broken vortex re-converges. As the impeller rotates, the vortex structure shifts to the suction side of the blade, and the vortex structure is in a constant state of breakup and coalescence.

#### 4.4.2 Unsteady Vorticity Analysis with Different Gas Content

With the intention of further analyzing the influence of impeller rotation on the spatio-temporal evolution of the inner vortex of the volute and impeller, the Z-direction vorticity distribution of the cut-water area and the impeller

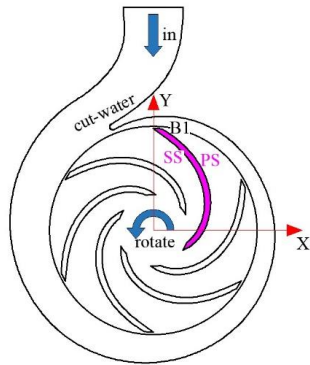


**Fig. 23 B1 region of the impeller**

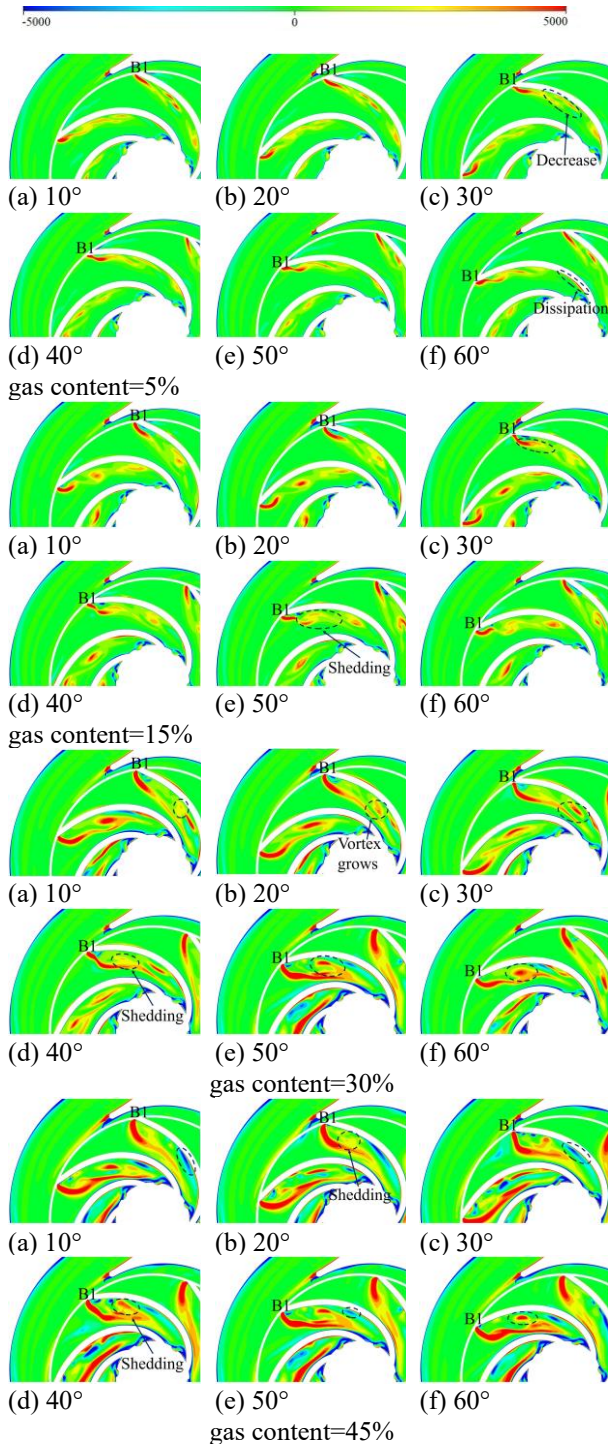


**Fig. 24 Vorticity at cut-water area and the impeller during rotation of B1**

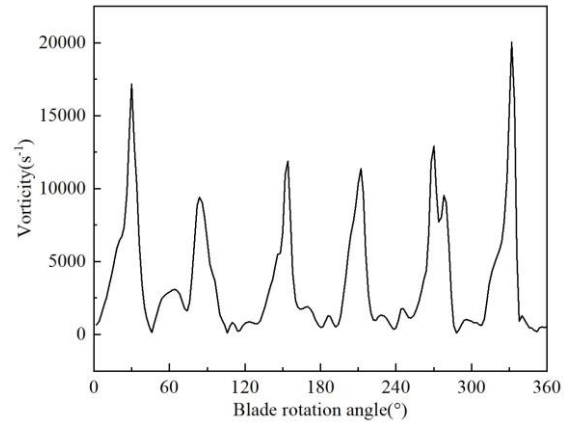


**Fig. 25 Vorticity of  $P_{gs4}$  variation with rotation at 45% gas content**

single channel under different gas content in the 1/6 impeller rotation period (blade B1 turns 60°) is compared. Where, the Z-direction vorticity is defined by the following formula:

$$w_z = \left( \frac{\partial u_y}{\partial x} - \frac{\partial u_x}{\partial y} \right) \quad (7)$$

The initial position of the volute and impeller blade B1 is presented in Fig. 23. The initial state is defined as the inlet center of the impeller flow channel on the suction side of the blade aligns with the volute cut-water. From Fig. 24, which shows the vorticity distribution of cut-water area and impeller single channel under different gas content in 1/6 impeller rotation period. Due to the strong wall shear effect of the fluid, a pair of vortices with opposite rotation directions appears at the leading edge of the cut-water. At 5% gas content, as the blade B1 rotates, the vortex at the blade wake leading edge gradually shifts moves to the blade wall. When the blade B1 turns 30°, the vortices at the position are merged, and the number of vortices decreases until the blade B1 turns 60°, and the vortices at the position are dissipated. At 15% gas content, with the rotation of blade B1, the vortex near the blade is gradually moved to the outlet of the impeller. The vortex at the wake of the blade gradually shifts to the outlet of the impeller. Starting from the blade B1 turning 30°, the vortex at the position is shown to fall off. When the blade B1 turns 50°, two vortices are completely separated. At 30% gas content, there is a vortex formation in the opposite direction at the trailing edge of the blade leading edge. With the rotation of blade B1, the vortex at the position of the blade B1 is gradually growing. When blade B1 turns 40°, A new vortex is shed at the graphic position and the shedding vortex grows with the rotation of blade B1 simultaneously. At 45% gas content, the area and number of vortices increase significantly. With the rotation of blade B1, new vortices fall off and grow continuously, and anti-directional vortices are generated in the middle edge of suction side. From blade B1 rotation 20° to 50°, the vortex length at this point is continuously shortened. The vortex length is the shortest at blade B1 rotation 50°, indicating that the vortex has reached the primary state at this time. In summary, the vortex evolution characteristics at the leading edge of the cut-water are substantially influenced by blade rotation. During blade rotation, there are new vortex shedding and growth, and some vortices

are gradually dissipated at the blade wall. In addition, the higher the gas content, the more pronounced the impact of blade rotation on the vortex evolution characteristics in the volute and impeller.

Figure 25 shows the change of vorticity at the monitoring point  $P_{gs4}$  with the rotation of the impeller. The findings indicate that vorticity exhibits periodic fluctuations, with the number of vorticity peaks corresponding to the number of blades. In addition, when the blade's leading edge is aligned with the cut-water, the vorticity is relatively large, and decreases as the blade distance from the cut-water. The fluctuation in vorticity during a cycle corresponds to the process shedding and regeneration of vortex.

## 5. CONCLUSION

Combined the reasonable numerical simulation and experiment method, the internal flow characteristics of the PAT with the gas content of 5 %, 15 %, 30 % and 45 % are studied respectively. Moreover, the unsteady pressure fluctuation and vorticity structure for spatio-temporal evolutionary properties under gas-liquid two-phase conditions are mainly investigated of the PAT. Overall, the main conclusions are as follows:

(1) The gas is mainly concentrated on the walls of the cut-water and the suction side of the blade. Influenced by the volute structure, significant gas-liquid separation is observed at the cut-water of the volute. The pressure value exhibits a decline along the direction of fluid flow. With the increase of gas content, the vortex size of each flow channel in the impeller increases, the volume fraction of gas-phase in each flow channel of the impeller increases obviously.

(2) The amplitude of pressure fluctuation in impeller and volute of the PAT increases with the increase of gas content under varying gas content conditions. In addition, the pressure fluctuation presents a periodic law inside the volute, and the blade frequency is the dominant frequency. Therefore, the primary reason for the periodic change of pressure fluctuation is the dynamic and static interference between the volute and impeller. At 5% gas content,  $P_{yde}$  rotation frequency ( $C_p=0.058$ ) at the impeller inlet exhibits a 3.5-fold increase compared to  $P_{ydl}$  at the outlet ( $C_p=0.017$ ). Channel blockage in the inlet area due to air mass agglomeration under high gas content conditions may explain the high main frequency fluctuation at the inlet monitoring point. As the impeller blade approaches the volute contraction section, pressure fluctuation in the blade channel increases due to volute shape. Since gas is mainly distributed on the suction side of the blade, where the flow field on becomes more complex, leading to increased amplitude.

(3) The vortex structure is mainly distributed in balance hole, inlet area of impeller and suction side of blade. During the revolution of impeller, the vortex structure on the blade suction side at different gas content gradually moves to the direction near the impeller inlet and the number of vortex structures decreases significantly. Due to the backflow at the volute outlet, vortices appear at some interfaces between the volute and the impeller, resulting in an increase in vorticity. The vortex evolution characteristics at the leading edge of the cut-water are

substantially influenced by blade rotation. In addition, with the rotation of the blade, there are new vortex shedding and growth, and some vortices are gradually dissipated at the blade wall. In addition, the higher the gas content, the more pronounced the impact of blade rotation on the vortex evolution characteristics in the volute and impeller.

## ACKNOWLEDGEMENTS

This work is supported by National Natural Science Foundation of China (52376036, 51906223, and U2006221), Science and Technology Key Plan Project of Xinjiang production and construction Corps (2021AA002), Science Foundation of Zhejiang Sci-Tech University (ZSTU)(23242147-Y).

## CONFLICT OF INTEREST

The authors declare that they have no known competing financial interests or personal relationships that could have appeared to influence the work reported in this paper.

## AUTHORS CONTRIBUTION

**J. Ying:** Writing, Conceptualization, Software; **H. Yang:** Writing - review & editing Supervision, Funding acquisition; **L. Li:** Visualization, Data curation; **X. Li:** Formal analysis, Methodology; **Y. Wei:** Investigation, Validation; **Z. Zhu:** Investigation, Guidance.

## REFERENCES

- Achitaev, A. A., Suslov, K. V., Nazarychev, A. N., Volkova, I. O., Kozhemyakin, V. E., Voloshin, A. A., & Minakov, A. V. (2022). Application of electromagnetic continuous variable transmission in hydraulic turbines to increase stability of an off-grid power system. *Renewable Energy*, 196, 125-136. <https://doi.org/10.1016/j.renene.2022.06.062>
- Adu, D., Du, J., Darko, R. O., Boamah, K. B., & Boateng E. A. (2020). Investigating the state of renewable energy and concept of pump as turbine for energy generation development. *Energy Reports*, 6, 60-66. <https://doi.org/10.1016/j.egy.2020.08.025>
- Bobba, K. M. (2006). Review of "vorticity and vortex dynamics". *AIAA Journal*, 44(12), 3166-3167. <https://doi.org/10.2514/1.27462>
- Chai, B., Yang, J., & Wang, X. (2022). Force characteristics of centrifugal pump as turbine during start-Up Process under gas-liquid two-phase conditions. *Actuators*, 11(12), 370-370. <https://doi.org/10.3390/ACT11120370>
- Chehadeh, D., Ma, X., & Al Bazzaz, H. (2023). Recent progress in hydrotreating kinetics and modeling of heavy oil and residue: A review. *Fuel*, 334. <https://doi.org/10.1016/j.fuel.2022.126404>
- Deen, N. G., Solberg, T., & Hjertager, B. H. (2001). Large eddy simulation of the Gas-Liquid flow in a square cross-sectioned bubble column. *Chemical Engineering Science*, 56(21), 6341-6349.

- [https://doi.org/10.1016/S0009-2509\(01\)00249-4](https://doi.org/10.1016/S0009-2509(01)00249-4)
- Feng, J., Zhao, N., Zhu, G., Wu, G., Li, Y., & Luo, X. (2023). Cavitation identification in a hydraulic bulb turbine based on vibration and pressure fluctuation measurements. *Mechanical Systems and Signal Processing*, 208, 111042. <https://doi.org/10.1016/j.ymsp.2023.111042>
- Furuya O. (1985). An analytical model for prediction of two-phase (Non condensable) flow pump performance. *Journal of Fluids Engineering, Transactions of the ASME*, 107, 139-147. <https://doi.org/10.1115/1.3242432>
- Hunt J. (1987). Vorticity and Vortex Dynamics in Complex Turbulent Flows. *Transactions of the Canadian Society for Mechanical Engineering*, 11(1), 21-35. <https://doi.org/10.1139/tcsme-1987-0004>
- Kandi, A., Meirelles, G., & Brentan, B. (2022). Employing demand prediction in pump as turbine plant design regarding energy recovery enhancement. *Renewable Energy*, 187, 223-236. <https://doi.org/10.1016/j.renene.2022.01.093>
- Li, D., Zuo, Z., Wang, H., Liu, S., Wei, X., & Qin, D. (2019). Review of positive slopes on pump performance characteristics of pump-turbines. *Renewable & Sustainable Energy Reviews*, 112, 901-916. <https://doi.org/10.1016/j.rser.2019.06.036>
- Lin, T., Zhang, J., Li, J., Li, X., & Zhu, Z. (2022). Pressure fluctuation-vorticity interaction in the volute of centrifugal pump as hydraulic turbines (PATs). *Processes*, 10(11), 2241. <https://doi.org/10.3390/pr10112241>
- Liu, M., Tan, L., & Cao, S. (2019). Theoretical model of energy performance prediction and BEP determination for centrifugal pump as turbine. *Energy*, 172, 712-732. <https://doi.org/10.1016/j.energy.2019.01.162>
- Lu, Z., Tao, R., Yao, Z., Liu, W., & Xiao, R. (2022). Effects of guide vane shape on the performances of pump-turbine: A comparative study in energy storage and power generation. *Renewable Energy*, 197, 268-287. <https://doi.org/10.1016/j.renene.2022.07.099>
- Mikielewicz, J., Gordon Wilson, D., Chan, T., & Goldfinch, A. (1978). A Method for correlating the characteristics of centrifugal pumping two-phase flow. *Journal of Fluids Engineering, Transactions of the ASME*, 100, 395-409. <https://doi.org/10.1115/1.3448698>
- Minemura, K., Uchiyama, T., Shoda, S., & Egashira, K. (1998). Prediction of air-water two-phase flow performance of a centrifugal pump based on one-dimensional two- fluid model. *ASME Journal of Fluid Engineering*, 120, (2), 327-334. <https://doi.org/10.1115/1.2820652>
- Osman, F. K., Zhang, J., & Lai, L. (2022). Effects of turbulence models on flow characteristics of a vertical fire pump. *Journal of Applied Fluid Mechanics*, 15(6), 1661-1674. <https://doi.org/10.47176/jafm.15.06.1303>
- Ouyang, J., Luo, Y., & Tao, R. (2021). Influence of blade leaning on hydraulic excitation and structural response of a reversible pump turbine. *Proceedings of the Institution of Mechanical Engineers, Part A: Journal of Power and Energy*, 236(2), 241-259. <https://doi.org/10.1177/09576509211034964>
- Qin, Y., Li, D., Wang, H., Liu, Z., Wei, X., & Wang, X. (2022). Multi-objective optimization design on high pressure side of a pump-turbine runner with high efficiency. *Renewable Energy*, 190, 103-120. <https://doi.org/10.1016/j.renene.2022.03.085>
- Shi, F., Yang, J., Miao, S., & Wang, X. (2019). Investigation on the power loss and radial force characteristics of pump as turbine under gas-liquid two-phase condition. *Advances in Mechanical Engineering*, 11 (4), 1-10. <https://doi.org/10.1177/16878140198437>
- Shi, F., Yang, J., Miao, S., Wang, X., Miao, S., & Guo, R. (2021). Study on the effect of gas-liquid two-phase medium on PAT performance: Original papers. *International Journal of Fluid Machinery and Systems*, 14(3), 247-257. <https://doi.org/10.5293/IJFMS.2021.14.3.247>
- Si, Q., Deng, F., Lu, Y., Liao, M., & Yuan, S. (2023). Unsteady cavitation analysis of the centrifugal pump based on entropy production and pressure fluctuation. *International Journal of Turbomachinery, Propulsion and Power*, 8(4), 46. <https://doi.org/10.3390/ijtp8040046>
- Stefanizzi, M., Torresi, M., Fornarelli, F., Fortunato, B., & Camporeale, S. M. (2018). Performance prediction model of multistage centrifugal Pumps used as Turbines with Two-Phase Flow. *Energy Procedia*, 148, 408-415. <https://doi.org/10.1016/j.egypro.2018.08.102>
- Wu, J., & Xue, F. (2021). *Cause analysis and treatment of slurry foaming in desulfurization absorption tower of 300MW unit*. IOP Conference Series: Earth and Environmental Science. <https://dx.doi.org/10.1088/1755-1315/804/3/032008>
- Yang, F., Li, Z., Yuan, Y., Lin, Z., Zhou, G., & Ji, Q. (2022a). Study on vortex flow and pressure fluctuation in dustpan-shaped conduit of a low head axial-flow pump as turbine. *Renewable Energy*, 196, 856-869. <https://doi.org/10.1016/j.renene.2022.07.024>
- Yang, S., Zhang, L., & Song, D. (2022b). Conceptual design, optimization and thermodynamic analysis of a CO2 capture process based on Rectisol. *Energy*, 244, 122566. <https://doi.org/10.1016/j.energy.2021.122566>
- Zhang, L., Li, Y., Zhang, Z., Chen, J., & Chen, D. (2022). Influence of blade number on performance of multistage hydraulic turbine in turbine mode. *Energy Science & Engineering*, 10(3), 903-917. <https://doi.org/10.1002/ese3.1070>